Observational- and modeling-based budget of lightning-produced NO_x in a continental thunderstorm

W. C. Skamarock, J. E. Dye, E. Defer, M. C. Barth, J. L. Stith, and B. A. Ridley
National Center for Atmospheric Research, Boulder, Colorado, USA

K. Baumann
Department of Space and Atmospheric Sciences, Georgia Institute of Technology, Atlanta, Georgia, USA

Received 4 February 2002; revised 22 November 2002; accepted 25 November 2002; published 21 May 2003.

[1] NO_x transport and production by lightning for the 10 July 1996 Stratosphere-Troposphere Experiment-Radiation, Aerosols, and Ozone convective storm is examined using radar, in situ observations and cloud model simulations. Observations and model simulations indicate that most of the NO_x produced by the storm was transported out into the anvil. The analyzed NO_x flux into the anvil, combined with results from a cloud model simulation, indicate that approximately 60 percent of the NO_x transported into the anvil during the observational period is produced by lightning. Lightning flash rate and channel length measurements, obtained using the Office National d'Etudes et de Recherche Arospatiales lightning interferometer, are combined with the NO_x budget to give estimates of average lightning NO_x production per interferometer flash and per unit flash channel length. The analysis yields production rates of approximately 43.2 moles (2.6×10^{25} molecules) NO_x per interferometer flash and 1.7×10^{-3} moles (1.0×10^{21} molecules) NO_x per meter of flash channel. These production rates fall within the bounds of rates derived in previous studies using completely different approaches. *INDEX TERMS:* 0320 Atmospheric Composition and Structure: Cloud physics and chemistry; 0368 Atmospheric Composition and Structure: Troposphere—constituent transport and chemistry; 3314 Meteorology and Atmospheric Dynamics: Convective processes; 3324 Meteorology and Atmospheric Dynamics: Lightning; *KEYWORDS:* lightning, NOx, convection, transport

Citation: Skamarock, W. C., J. E. Dye, E. Defer, M. C. Barth, J. L. Stith, B. A. Ridley, and K. Baumann, Observational- and modeling-based budget of lightning-produced NO_x in a continental thunderstorm, *J. Geophys. Res.*, *108*(D10), 4305, doi:10.1029/2002JD002163, 2003.

1. Introduction

[2] Nitrogen oxides (NO_x = NO + NO_2) are important reactive species in the photochemistry of the troposphere [*Bradshaw et al.*, 2000]. Currently, production of NO_x by lightning represents a large uncertainty in the global NO_x budget with estimates varying by up to two orders of magnitude, although the range is likely within 2–20 Tg(N)/yr [*Liaw et al.*, 1990; World Meteorological Organization (*WMO*), 1995; *Huntrieser et al.*, 1998]. The uncertainty is amplified for global models of tropospheric processes because lightning-produced NO_x can be a direct source to the middle and upper troposphere where its lifetime is considerably longer than in the boundary layer. Estimates of the global budget of lightning-produced NO_x (LNO_x) rely on a number of assumptions that lead to this large uncertainty [e.g., *Price et al.*, 1997; *Lawrence et al.*, 1995]. For example, there is an incomplete understanding of the physics of NO_x production by the different components of a lightning flash and uncertainty associated with quantitatively characterizing the lightning discharge energy and channel length in convective storms. Further uncertainty arises in the extrapolation of lightning flash characteristics and storm production rates to the global LNO_x budget.

[3] As a step toward quantifying and reducing the uncertainty in the LNO_x budgets, the assumptions and parameters used in these models should be compared with direct observations where possible. Toward this end, we present an NO_x budget for a continental thunderstorm observed on 10 July 1996 during the Stratospheric-Tropospheric Experiment: Radiation, Aerosols, and Ozone (STERAO)/Deep Convection project. In this study we use detailed measurements of lightning flash rates and channel lengths of lightning components to examine NO_x production by lightning. The budget includes estimates of the time varying lightning production rate of NO_x, total lightning NO_x production over the lifetime of the storm, and estimates of the average NO_x production per flash and per meter flash channel length during the storm. These budget products can be directly compared with parameters used in global LNO_x budgets and with estimates from other observational, laboratory and theoretical studies.

[4] The budget is produced by combining meteorological and chemical observations from aircraft in the anvil outflow (section 2), an analysis of NO_x transport in a 3D cloud-

0148-0227/03/2002JD002163

model simulation of the storm (also in section 2), and measured lightning flash rates and estimated lightning channel lengths using data from the ONERA lightning interferometer (section 3). Extrapolation of these results to the global scale is considered in the last part of section 3, followed by a summary and discussion in section 4.

2. NO_x Flux Analysis

[5] The 10 July STERAO storm developed along the southern portion of the border between Wyoming and Nebraska over a locally elevated topographic feature known as the Cheyenne ridge. Through most of its lifetime (from approximately 2200 GMT 10 July to 0100 GMT 11 July, or 1600 to 1900 10 July local time) the convective system consisted of multiple cells aligned along a NW-SE axis. Storm inflow at low levels was from the south and west, and anvil outflow was to the SE in the lower and middle parts of the anvil (from 6.5 to 10.5 km MSL) and toward the east above approximately 12.5 km MSL. The orientation and growth of the anvil are dictated by the upper level winds, which were northwesterlies turning to westerlies above 12.5 km, and by the slow storm movement relative to these upper level winds (approximately 5 m/s toward the SSE [*Skamarock et al.*, 2000]. After 0100 GMT 11 July, the storm consisted of a single strong cell (with supercell characteristics) that propagated at a somewhat higher speed to the south.

[6] Extensive observations of the storm were obtained from a variety of platforms [see *Dye et al.*, 2000]. Of particular interest for this study, NO, CO and ozone measurements were taken on the North Dakota Citation aircraft [*Stith et al.*, 1999; *Dye et al.*, 2000] while it flew through the anvil of the storm. Figure 1 shows the projection of the Citation flight track between 2313 10 July and 0040 GMT 11 July on the horizontal plot of radar reflectivity (at 00 GMT 11 July) at 10.5 km MSL. The Citation aircraft mapped out the anvil structure during this time period by traversing the anvil in horizontal passes, approximately perpendicular to the long axis of the anvil, at elevations starting at approximately 11.8 km MSL (close to the anvil top) and ending at approximately 6.8 km MSL. Both satellite photos and radar reflectivity [see *Dye et al.*, 2000; *Skamarock et al.*, 2000, Figure 5] suggest that the evolution of the storm from a line of convective cells to a single supercell occurred somewhat after the period in which the Citation observations in the anvil were taken. Based on the mean upper level winds, a parcel detraining from the core into the anvil would take around 45 minutes to reach the area in which the Citation was flying. Thus the aircraft was sampling anvil air from the multicellular period of the storm, detrained from the updrafts from between approximately 2230 GMT 10 July to 00 GMT 11 July.

[7] Visible satellite images of the storm at 2315 10 July and 0015 11 July (Figure 2) suggest that the primary changes in the storm between these times are growth of the anvil to the southeast and east along with a propagation of the convective line to the south. Radar reflectivity plots (see Figure 1 and *Skamarock et al.* [2000]) show that between 2 to 4 cells were active in the convective line at any time during this period. Given that the area of active convection does not grow significantly relative to the

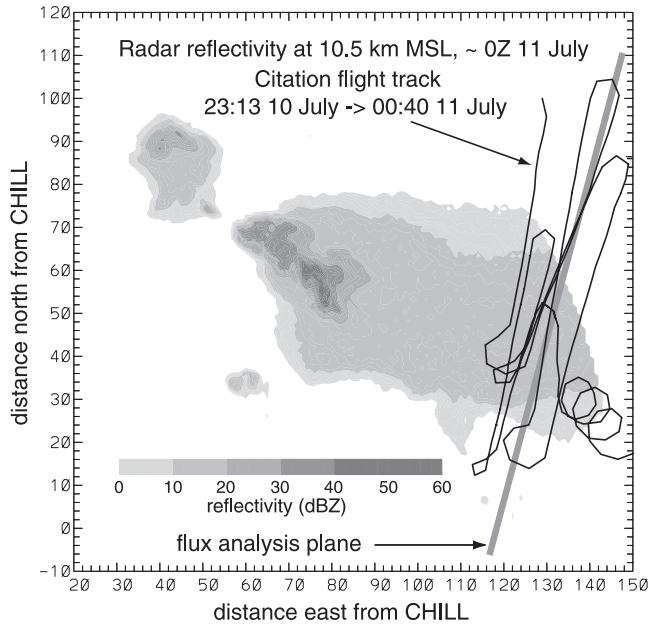

Figure 1. Horizontal cross section of radar reflectivity at 10.5 km MSL. The analysis plane is shown in the thick gray line and the black line is the aircraft flight track.

growth of the anvil area, it is likely that the growth of the anvil represents the net convective detrainment during this time period. Observations of NO, CO and O_3 taken on the Citation aircraft allow us to compute these fluxes (the convective detrainment) into the growing anvil.

[8] Because the Citation obtained measurements of NO and not NO_x, we perform the flux analysis on measured NO mixing ratios and then determine the flux of NO_x using the photochemical steady state assumption. For this assumption we consider only the NO, NO_2, and O_3 chemistry such that the NO_2 to NO ratio is $[NO_2]/[NO] = k_2\,[O_3]/j_1$, where j_1 is the photolysis frequency of NO_2 which produces NO and $O(^3P)$, and k_2 is the rate constant of the NO + O_3 reaction. We calculate the NO_2 to NO ratio to be 0.3 for clear sky conditions in the upper troposphere. In the upper part of the anvil where photolysis frequencies are enhanced by cloud scattering by a factor of two or so, the NO_2 to NO ratio could be half the clear sky value, while in the optically thick lower portion of the anvil the NO_2 to NO ratio would be larger. In addition, departure from the photochemical steady state due to peroxy radicals would also increase the NO_2 to NO ratio. However, lightning-produced NO in the anvil will decrease the NO_2 to NO ratio. Thus, we estimate that the NO_x to NO ratio could range from 1.1 to 1.6 [*Dye et al.*, 2000], and we use a constant value of 1.3 in the remainder of the analysis.

2.1. Control Volume Analysis

[9] We perform a flux analysis for the 10 July storm in order to quantify the net detrainment of air mass, NO_x and CO, with the goal of relating the NO_x flux to lightning NO_x production. The flux analysis can be understood by considering the 2D depiction of a generic storm (Figure 3) in which a control volume is drawn around the storm. The time rate of change of NO_x mass in the control volume will be the difference between the inflow and outflow through the

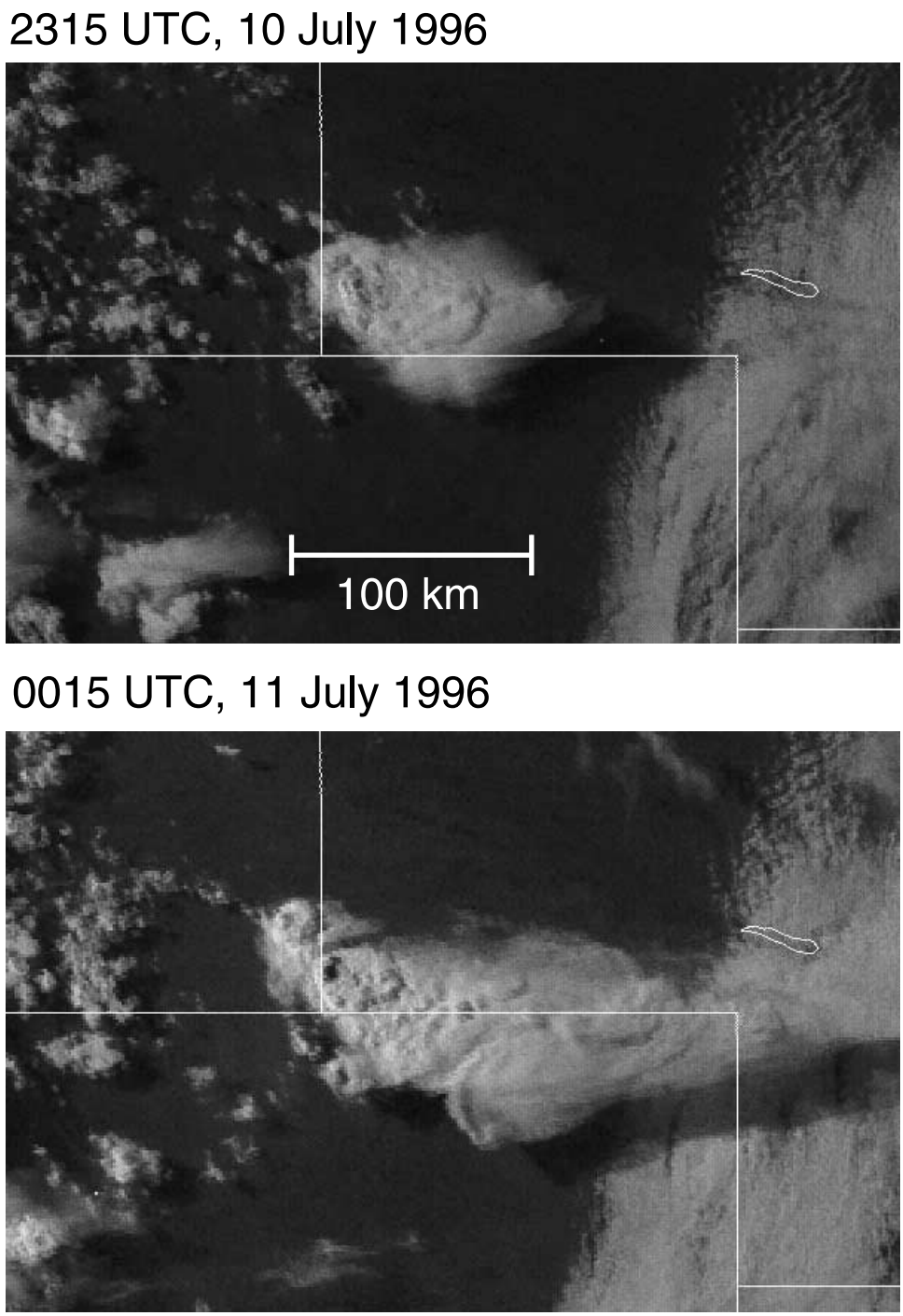

Figure 2. Visible satellite images of the storm at 2315 GMT 10 July 1996 and 0015 GMT 11 July 1996.

control volume boundary plus any sources within the volume. This is quantitatively stated by the conservation equation

$$\int_V \frac{\partial \rho \phi_{NO_x}}{\partial t} = \int_\Gamma \left(\rho \mathbf{v} \cdot \mathbf{n} \, \phi_{NO_x} \right) + S_{NO_x}, \qquad (1)$$

where ρ is the dry air density, ϕ_{NOx} is the NO_x mixing ratio with respect to the dry air, V is the control volume, Γ is the control volume boundary, v is the velocity, n is the unit normal to the boundary Γ, and S_{NOx} is an NO_x source. All the terms are time-dependent.

[10] Generally, all the terms in equation (1) can be significant. The Citation aircraft measured only part of the first term on the RHS of (1), that being the flux of NO_x out into the growing anvil. We have no measurements of the flux of NO_x from the boundary layer into the storm or downdraft fluxes of NO_x out of the storm (i.e., other major contributions to the second term in (1)). We also have no direct measurements of NO_x production by lightning in the

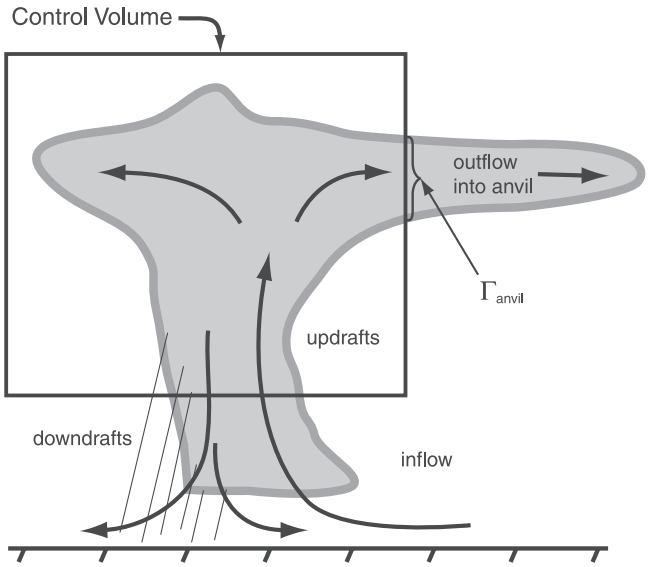

Figure 3. Two-dimensional conceptualization of a storm along with the control volume used for the flux analysis.

storm (the source term), and we have no direct measurements of the change of NO_x storage inside the control volume (within the storm, the leftmost term).

[11] For the 10 July storm, indirect evidence strongly suggests that the leftmost term in (1) is small relative to the other terms in the equation and that most of the NO_x produced by lightning is ultimately detrained into the anvil. The arguments and evidence that support these assumptions are as follows:

[12] 1. As noted previously, the area of active convection did not change significantly in size relative to the change in size of the anvil over the period of the Citation anvil traverses. This is supported by visible imagery (Figure 2), and the radar reflectivity [see *Dye et al.*, 2000; *Skamarock et al.*, 2000].

[13] 2. There is little evidence suggesting that convective downdrafts, which were generally weak, were transporting significant quantities of NO_x (either lightning produced NO_x or NO_x previously transported upward from the PBL by convection). Specifically, the NOAA P3 aircraft saw little enhancement in NO below the anvil or at lower levels in the vicinity of the storm, and lightning was observed to occur mostly within moderate updrafts, and not within strong downdrafts [*Dye et al.*, 2000]. Additionally, modeling results suggest that downdrafts reaching the boundary layer are likely to have their origins below approximately 5.5 km MSL [*Skamarock et al.*, 2000]; this is below the level where most of the lightning was observed in this storm.

[14] 3. Comparison of lightning locations with Doppler radar derived fields of vertical velocity showed lightning occurring mostly in regions of moderate updraft [*Dye et al.*, 2000].

[15] 4. The lightning was almost all intercloud (IC) [*Dye et al.*, 2000; *Defer et al.*, 2001] and the strong storm-relative upper level winds should advect most of the lightning-produced NO_x through the anvil.

[16] These arguments and evidence suggest that it is reasonable to dispense with the storage term in (1) and to assume that all the NO_x produced by lightning is ultimately detrained into the anvil. These two assumptions allow us to focus the flux analysis on the flux into the anvil through the boundary subregion Γ_{anvil} in Figure 3. The assumption that all lightning-produced NO_x fluxes out into the anvil can be stated as

$$S_{NO_x} = -\int_{\Gamma_{anvil}} \left(\rho V \cdot \mathbf{n}\phi^S_{NO_x}\right), \tag{2}$$

where ϕ^S_{NOx} is the lightning-generated NO_x. The Citation aircraft observations, however, measure the total flux of NO out into the growing anvil, allowing us to estimate the NO_x flux, i.e.,

$$-\int_{\Gamma_{anvil}} \rho V \cdot \mathbf{n}\,(\phi^E_{NO_x} + \phi^S_{NO_x}), \tag{3}$$

where ϕ^E_{NOx} is the pre-existing (environmental) NO_x. We cannot distinguish between lightning produced NO_x and, say, that transported upward from the boundary layer by updrafts or entrained directly into the anvil flow from the environment. We must disentangle the two fluxes in (3) in order to compute the NO_x production rate from lightning, S_{NOx} in (2). We will use results from a cloud model simulation of the 10 July storm to estimate the amount of NO_x transported into the anvil that accounts for all the flux except that of lightning-produced NO_x. The remaining NO_x flux through the anvil can be attributed to the lightning produced NO_x and thus is an estimate of the lightning NO_x production S_{NOx} in (2). In the remainder of this section we analyze the total flux using the observations from the Citation, estimate the flux of pre-existing NO_x (ϕ^E_{NOx}) from the cloud model simulation, and combine the two fluxes to extract the lightning NO_x production rate S_{NOx}.

2.2. Objective Analysis of Aircraft Observations

[17] Figure 4a depicts the Citation aircraft track projected perpendicularly onto the vertical flux analysis plane (whose location is shown in Figure 1). The analysis plane moves with the storm at the system velocity (u, v) = (1.5, −5.5) m/s where u is positive toward the east and v is positive toward the north [see *Skamarock et al.*, 2000]. Observations from the Citation aircraft are averaged over 30 sec intervals and likewise projected onto the analysis plane, and include the horizontal winds (u,v), NO, CO, O_3 and cloud particle concentration from the Particle Measuring Systems 2D probe [see *Dye et al.*, 2000]. The location of the midpoints of the 30 sec averages are shown as circles along the flight track in Figure 4a. The CO data is necessarily time averaged because of the response characteristics of the CO instrument [see *Dye et al.*, 2000], the other observations are averaged in the same way for consistency. In the analysis that follows, the time-averaging does not significantly affect on the results.

[18] For calculating fluxes, the projected observations are analyzed onto a regular grid (Δx = 2000 m, Δz = 200 m) using an objective analysis procedure similar to that developed by *Cressman* [1959]. In this application we represent a variable as the sum of a reference state and a perturbation, $\phi = \phi_o(z) + \phi'$, where the reference state represents the undisturbed (pre-convective) environment. On the regular grid at

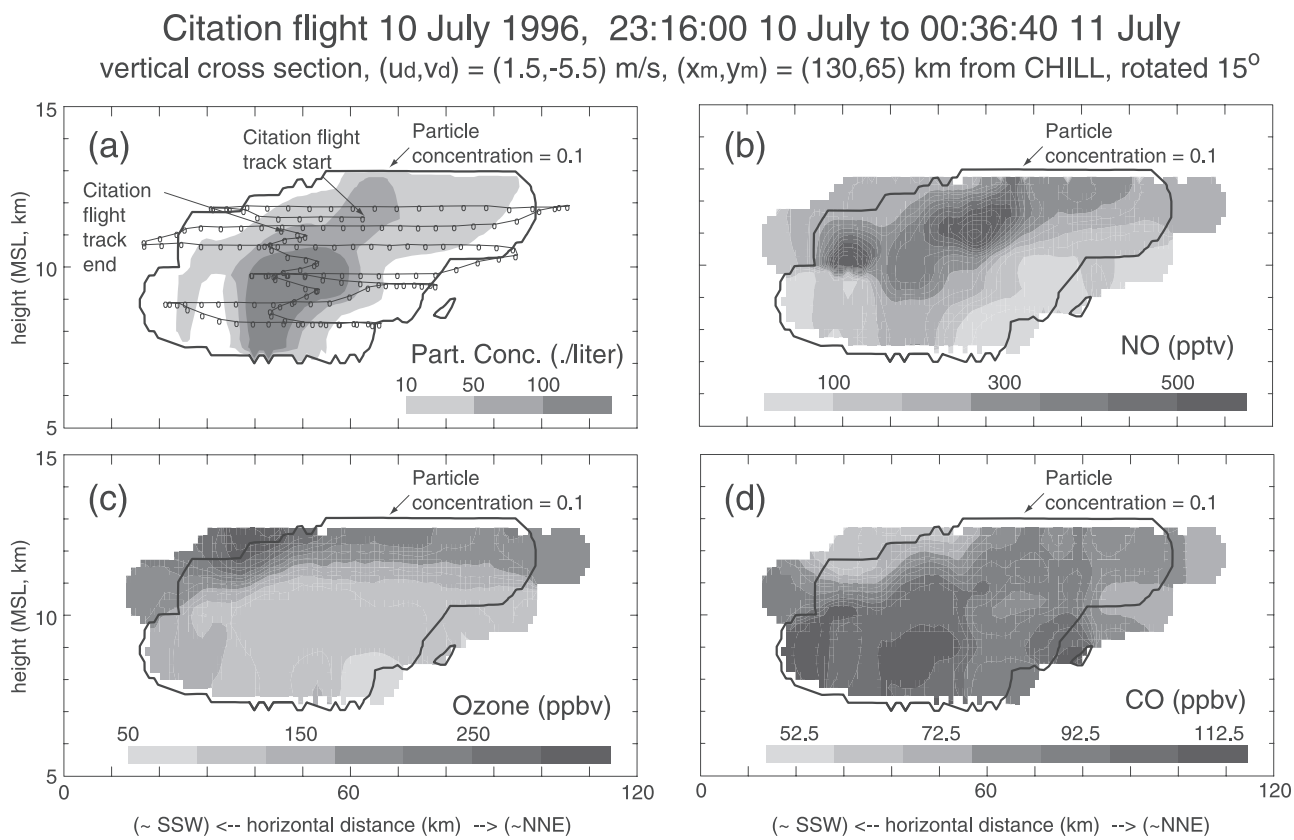

Figure 4. Objective analysis of (a) cloud particle concentration, (b) NO, (c) O_3, and (d) CO using the Citation flight data. The flight track is shown in the cloud particle concentration plot. See color version of this figure at back of this issue.

points (z_a, x_a) we calculate the objectively analyzed value $\phi_a = \phi_o(z) + \phi'_a$ by computing the perturbation value ϕ'_a using

$$\phi'_a = \frac{\sum_{i=1}^{K} w_i(\phi_{obs} - \phi_o(z))}{\sum_{i=1}^{K} w_i},$$

where

$$w_i = \frac{1 - d^2}{1 + d^2}, \quad if \quad d^2 < 1,$$

$$w_i = \frac{1 - d^2}{1 + d^2} 0, \quad if \quad d^2 \geq 1,$$

and

$$d^2 = \left(\frac{x_a - x_{obs}}{x_r}\right)^2 + \left(\frac{z_a - z_{obs}}{z_r}\right)^2.$$

[19] The observed values are denoted as $\phi_{obs}(z_{obs}, x_{obs})$, and x_r and z_r define the radius of influence of the observation on the analyzed values, which in our analyses are $x_r = 5$ km and $z_r = 1.5$ km. The results of the following flux analysis are not sensitive to values of x_r and z_r, and the primary constraint on the values are that z_r be significantly greater than half the height difference between flight levels (>1/2 km), and x_r be significantly greater than half the horizontal distance between time-averaging locations. Neither are the results sensitive to the analysis grid lengths Δx and Δz. The results are also relatively insensitive to the choice of reference states; the reference states from *Skamarock et al.* [2000] are employed here for the horizontal winds (u,v), CO and O_3. The reference state for NO (and CO and O_3) can be found in Figure 5, and the background cloud particle concentration is zero.

[20] Figure 4 presents the results from the objective analyses for NO, CO and O_3, along with cloud particle concentrations from the 2D probe. The data are contoured only where observations have contributed to the values. The analyzed fields extend somewhat more than a km above and below the highest and lowest flight track observations. We have no data in these regions and the values represent an extrapolation.

[21] The fields possess much structure. First, the tropopause is clearly depicted in the O_3 field, where a significant dip in the tropopause is evident at the top southwest edge of the anvil. This signature is also evident in the CO analysis. The structure can differ substantially between fields. For example, the NO analysis shows isolated maxima located above 10 km MSL while the CO analysis shows somewhat less-isolated maxima located below 10 km MSL. Two factors likely contribute to the different structures; the preconvective vertical distributions of NO and CO differ (higher CO levels extend well beyond the PBL top compared to NO, see Figure 5), and NO is also produced by lightning. The two maxima of NO >500 pptv are likely major out-flux areas of LNO_x.

[22] To compute fluxes of mass and other species through the anvil on the analysis plane, we use the plane-perpendicular velocities analyzed from the aircraft data (not shown) along with the analyzed NO and CO and a reference density profile. We define the anvil area as the area within the 0.1

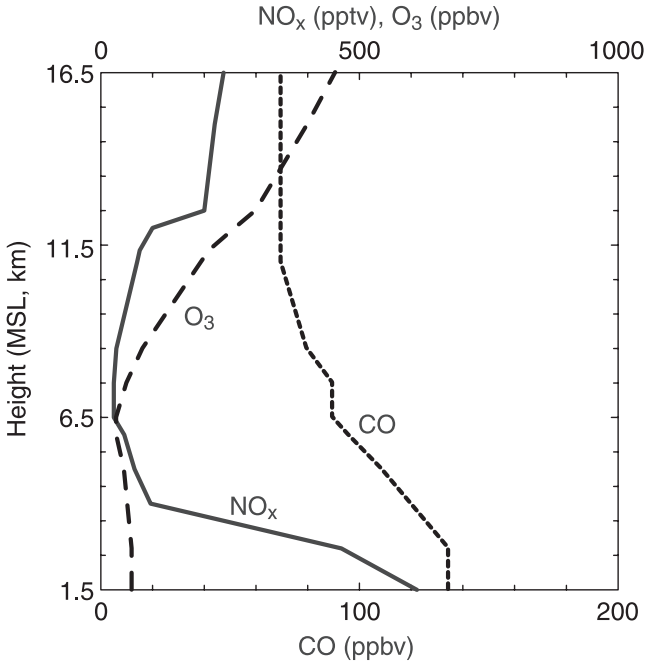

Figure 5. Environmental profile of NO_x, CO and O_3 used in the cloud model simulation.

particles per liter contour in the particle concentration analysis in Figure 4a. The resulting fluxes are given in Table 1. Next, we use a cloud model simulation that includes passive tracer transport to partition the NO_x fluxes in (3).

2.3. Cloud Model Simulation

[23] A three-dimensional cloud model simulation of the 10 July storm is described by *Skamarock et al.* [2000]. The simulation, performed using a horizontally homogeneous environment and thermodynamic and wind soundings composited from the STERAO observations, generally reproduced the observed structure and evolution of the storm. A comparison of the simulated convective system with observations and a detailed analysis of CO and O_3 transport in the storm was performed by *Skamarock et al.* [2000]. To produce the flux analysis, we have repeated the simulation using a larger horizontal domain to better capture the growing anvil (160 $\times$ 160 km), and we have included another passive tracer representing NO_x in addition to CO and O_3. There is no lightning source of NO_x in the model, hence the NO_x in the model represents NO_x existing in the pre-storm environment. The environmental CO profile is given by *Skamarock et al.* [2000] and is shown in Figure 5. The environmental NO_x profile, also shown in Figure 5, is derived from aircraft observations and climatology. NO measurements obtained from the WP3D aircraft were averaged at model levels up to 6.5 km MSL. The standard deviation of these averages was approximately 40% of the mean value. The NO_x mixing ratios were computed by assuming a photochemical steady state for O_3, NO, and NO_2 chemistry (again peroxy radicals were not included in the photochemical steady state calculations). The NO_2 photolysis rate used in the calculation of the photochemical steady state was determined from radiometric measurements made on the WP3D [*Frost et al.*, 1998]. The NO_x mixing ratios for the 6.5–14 km MSL altitudes were obtained from the UND Citation out-of-cloud NO measurements averaged at model levels and adjusted to NO_x values using the photochemical steady-state assumption. Above 14 km MSL, NO_x mixing ratios were determined by using NO_x data reported in the literature [*Salawitch et al.*, 1994] and mean July NO_x mixing ratios as calculated by the global chemistry transport model MOZART [*Brasseur et al.*, 1998] for the grid point (104.1°W, 40.5°N) nearest to northeastern Colorado.

[24] Figure 6 shows a horizontal cross section of radar reflectivity derived from the model output at 6000 sec in the simulation, and can be compared with Figure 1. The position of a vertically oriented analysis plane, comparable to that used in the analysis of the aircraft observations, is also shown in Figure 6. The location of this plane is chosen such that it is a similar distance downwind of the convective cells compared with the plane used for the observational analysis.

[25] Figure 7 shows an outline of the model cloud field and NO_x, and it can be compared with the observational analysis of NO in Figure 4. Several differences are obvious in the comparison. First, the simulated anvil cross-sectional area is significantly smaller than that observed, averaging less than two thirds the observed area through most of the simulation. We attribute this to the fact that the simulated convection produced a somewhat smaller system than that observed; convective cells were triggered or regenerated somewhat more readily in the observed storm than in the simulation. Second, the simulation does not exhibit the pronounced

Table 1. Flux Analysis for the Observations and Simulation

	Cross Section Area, $10^6 m^2$	Dry Air Mass Flux Density, $kg/s/m^2$	CO Flux Density, 10^{-5} moles/s/m^2	NO_x Flux Density, 10^{-8} moles/s/m^2
Observations (Citation data)	315	5.9	1.9	4.5 (NO) 5.8 (NO_x) (NO_x = 1.3*NO)
Simulation Time (s)				
3600	109	6.7	1.9	2.4
4200	177	6.6	1.9	2.2
4800	193	6.5	1.9	2.2
5400	232	6.6	1.9	2.3
6000	238	6.5	1.9	2.2
6600	187	6.6	2.0	1.9
7200	119	6.5	2.0	2.0
Average of the 7 times	180	6.6	1.9	2.2

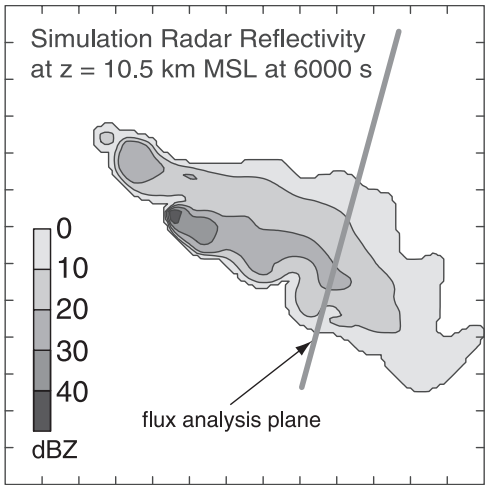

Figure 6. Horizontal cross section of radar reflectivity from the cloud model simulation at 6000 sec. The location of the analysis plane used for the simulation is also included.

peaks of NO_x in the upper part of the anvil found in the observational analysis of NO. We attribute this to the presence of lightning-produced NO_x in the observations.

[26] Fluxes of air mass, CO and NO_x integrated over the anvil through the analysis plane have been computed. For quantitative comparison we have computed the flux densities (fluxes divided by the anvil cross-sectional areas) and these flux densities are presented in Table 1. The simulated fluxes are given at ten minute intervals between 1 hour and 2 hours. This period corresponds to a time somewhat before the simulated storm transitions to a supercell. The observations used to compute the fluxes span a little over an hour starting at approximately 2315 GMT, somewhat before the observed storm transitioned to a supercell. We have chosen to sample the simulation so that the storm character during the period used for the simulation analysis corresponds to the observed storm's character for the time during which the aircraft data used in the observational flux analysis were taken.

[27] The mass and CO flux densities compare well, although the air mass flux density is consistently approximately 10% higher than the observed mass flux density. This difference could be attributed to errors in the initial wind profile or other errors in the convective simulation. The average normalized NO_x fluxes differ dramatically. The observed flux density is approximately 2.5 times larger than the simulated flux density. From this we conclude that somewhat over 60 percent of the observed NO_x flux out the anvil can be attributed to lightning-generated NO_x. This results in an average of approximately 11.5 moles/s (6.9×10^{24} molecules/s) NO_x produced by lightning (anvil area $\times$ NO_x flux per unit area $\times$ 0.62) transported through the anvil cross section during the observation period.

[28] There are a number of possible sources of error in this flux analysis. In the cloud model simulation, the distribution of NO_x in the simulated anvil is moderately sensitive to the environmental profile (see Figure 5). Decreasing the NO_x in the upper troposphere in the profile leads to a small increase in LNO_x production (70% of the flux is attributed to LNO_x if the upper level environmental NO_x is specified as 50 pptv). Likewise decreasing the

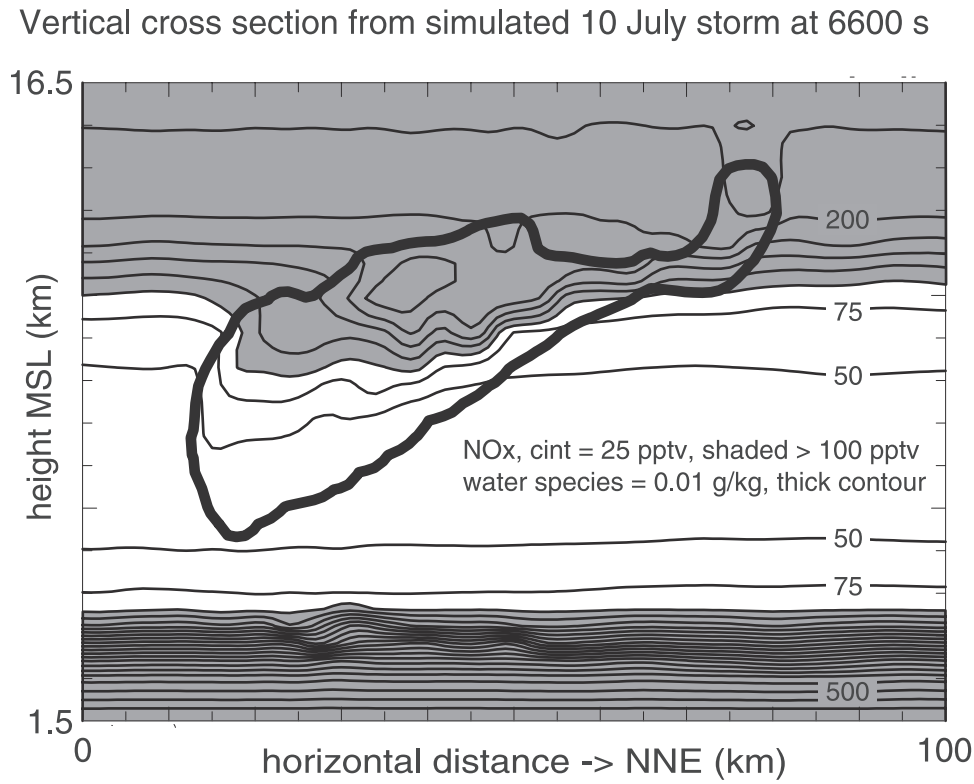

Figure 7. Vertical cross section of NO_x and water species in a position similar to the analysis cross section.

boundary layer NO_x leads to an increase in LNO_x production. With respect to the observational analysis and apart from the assumptions discussed previously concerning the control volume and storm evolution, there is the issue of how to characterize the objective analysis of the aircraft data given that the storm was evolving over the time during which the anvil was mapped. Specifically, while the average of the fluxes from the simulation result in a definable time average, the observations from the anvil do not constitute a similar time average. The assumption we implicitly make in using the observations in this analysis is that this snapshot of the anvil structure is representative of the actual time-averaged anvil structure. Radar reflectivity plots (not shown) suggest that the anvil cross-sectional area did not vary dramatically over the observational period-much less than the factor of 2 found in the simulation. Furthermore the values of NO, CO and O_3 measured during the spiral ascent at the end of the observation period are comparable to those from the previous horizontal pass at the different altitudes. The simulation also suggests that the flux densities do not vary much during the sampling period; the simulated flux densities of NO_x, CO and mass vary by less that ±10% even though the anvil cross-sectional area varies by a factor of 2. These results suggest that our assumption of the representativeness of the anvil objective analysis may be reasonable.

3. Lightning and NO_x Production

[29] In the following section we produce estimates of the average LNO_x production per unit channel length and per flash, and total storm LNO_x production based on total lightning channel length produced by the storm (i.e., the sum of all lightning-component lengths) and total flashes, under the assumption that all lightning-produced NO_x appears in the anvil outflow. Support for this assumption was outlined in the previous sections: The storm produced mostly IC lightning as opposed to CG lightning during the analysis period (2230–2400 GMT), the P3 aircraft did not find evidence of enhanced NO_x values at low levels, and the multiple Doppler analyses did not show lightning occurring in pronounced downdrafts. Also, simulations we have performed with NO_x sources used to simulate lightning production (distributed over a broad altitude and horizontal area) show LNO_x being primarily transported out into the anvil.

[30] Estimates of the lightning channel lengths and flashes are derived from data obtained by the ONERA lightning interferometer. The interferometer was deployed to record the total lightning activity in the observed convective storms. The capabilities of the instrument and the analysis of the data for the 10 July storm are described by *Defer et al.* [2001], which includes a description of the methods used to determine lightning flashes. Flash reconstruction is accomplished by examining the time and spatial location of VHF pulses recorded by the interferometer. A VHF source is associated with a flash if the azimuth and elevation (as measured by the interferometer) of the VHF source is spatially and temporally close to those of the previous sources already considered part of the flash. For example, temporally, if the time between 2 sources was more than 500 ms, the second source is considered the start of a new flash. The determination of spatial closeness is somewhat more involved and we refer the reader to *Defer et al.* [2001]. The methods used to estimate the length of the flash components are described by *Defer et al.* [2003]. We want to emphasize that our flash rates and channel lengths are different from those used in previous studies. The flash rate includes all flashes detected by the interferometer that had durations ranging from 23 μ sec (the shortest duration measurable by the interferometer) to over 1 sec. Likewise the total channel length is an estimate of the sum of lengths of the negative leaders, K changes and return strokes.

[31] In this study we assume that all the components radiating in the VHF domain take part in the LNO_x production. Analysis of the VHF radiation during the period 2230–2400 indicated that most of the flash components were K change processes [*Defer et al.*, 2001], which are likely to have temperatures in excess of 20,000 K, similar to dart leaders [*Orville*, 1975] and well above the NO freeze-in temperature of 3500 K [*Chameides et al.*, 1977]. Very few negative leader processes were recorded during this period probably due to their weak signal at the lightning mapper stations.

3.1. Lightning NO_x Production Rate

[32] A flash-by-flash analysis has been performed in order to characterize the interferometer flash rate and flash durations for the entire storm [*Defer et al.*, 2001]. *Defer et al.* [2003] applied simple relations to estimate the total length of all the flash components radiating in the VHF domain, relations deduced from the physics of lightning. The lightning component channel length production rate and the interferometer flash rate from this analysis are given in Figure 8 for the entire life of the storm. Both interferometer flash rate and component channel length production rate vary significantly during the storm. These two measures of lightning activity are not always well correlated, evidence the large peak at approximately 2320 UT in the interferometer flash rate that does not correspond to a particularly large peak in component channel length production. In fact, analysis of the flash population reveals that at about 2320 UT, half of the flashes had durations less than 1 ms [*Defer et al.*, 2003]. Many of these short duration flashes emitted intense VHF radiation suggestive of large currents and temperatures. The flash lengths shown here are very different and much longer then those estimated or assumed in previous studies of lightning produced NO_x [e.g., *Price et al.*, 1997] where emphasis was on CG return strokes. Likewise the overall flash channel length production is orders of magnitude larger than estimates discussed in previous studies.

[33] The average lightning channel length production rate over the period 2230 GMT to 2400 GMT is approximately 6700 m/s (see Figure 8). Using the analyzed lightning production rate for NO_x given in the previous section, we estimate that the average amount of NO_x produced per meter path length over this period is approximately 1.7×10^{-3} moles/m NO_x (1.0×10^{21} molecules/m NO_x).

[34] This estimate of NO_x production rate per meter channel length falls within other NO_x production rate estimates produced using entirely different approaches. *Stith et al.* [1999] analyzed NO_x peaks encountered along the flight track from the STERAO storms on 9, 10 and 12 July 1996. In that study, individual NO spikes (above a measured background) were fit to a simple model of lightning generated NO plumes. Using the model, they estimate that

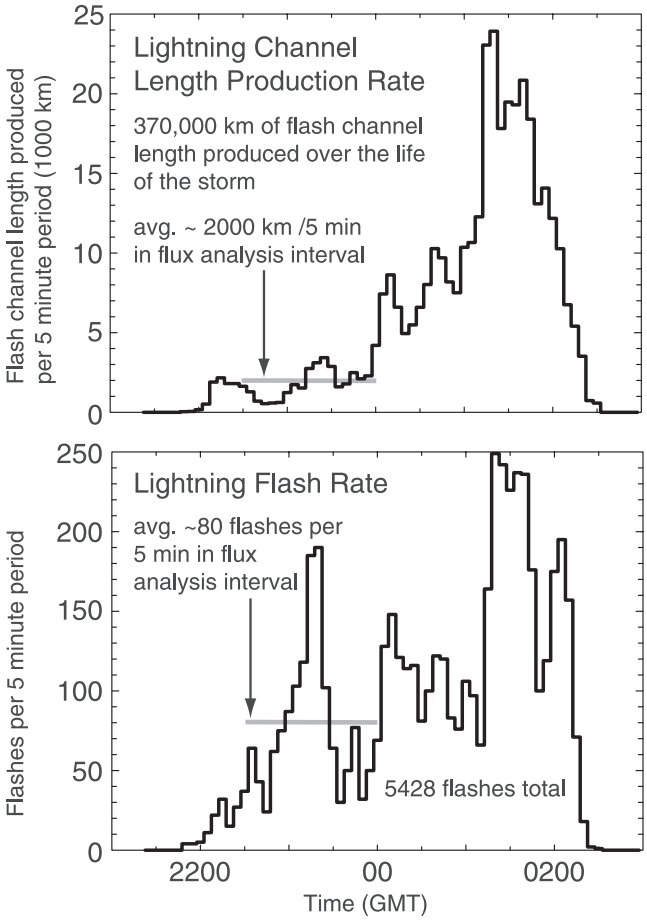

Figure 8. Lightning channel length production and flash rate for the 10 July STERAO storm. Data from *Defer et al.* [2003].

between 2×10^{20} and 10^{22} molecules of NO_x per meter were produced in the plumes that they sampled. The large range found by Stith et al. and also by *Huntrieser et al.* [2002] for a storm in Germany suggests that different channels of a lightning flash may produce varying amounts of NO_x. Our estimate (1.0×10^{21} molecules NO per meter), which integrates the NO_x over the storm outflow and uses estimates of total lightning channel length, is in the lower end of the *Stith et al.* [1999] range, suggesting that on average many channels are weak producers of NO_x. *Wang et al.* [1998] found between 5×10^{20} and 3×10^{21} molecules of NO_x per meter of flash channel were produced for lightning generated in the laboratory at sea level with currents between 10 to 30 kA, which are comparable to currents observed in the return strokes of negative CG lightning. Our estimate of LNO_x production falls in the lower end of the *Wang et al.* [1998] range. While IC lightning is assumed to have low peak currents (a few kA) relative to CG flashes, our results and those of *Stith et al.* [1999] and *Huntrieser et al.* [2002] suggest that IC lightning is producing significantly more NO_x than expected from simple scaling of the *Wang et al.* [1998] results using peak currents and pressure. This discrepancy suggests that peak currents in IC lightning may be higher, or that some other aspect of NO_x production in IC lightning is not understood.

[35] Flashes are also determined from the interferometer data, and can be used to compute LNO_x production per flash. Over the period from 2230 GMT to 2400 GMT, the average interferometer flash rate was approximately 0.27 flashes per second for flashes with durations from 23 μ sec to over 1 sec. Combining this flash rate with the LNO_x production rate leads to an average LNO_x production rate per flash of 43.2 moles/flash (2.6×10^{25} molecules/flash). This estimate of NO_x production per flash is consistent with existing estimates. *Lawrence et al.* [1995], in a review of previous theory, laboratory experiments and observational analyses of mostly CG flashes, found that between 0.5 to 300×10^{25} molecules of NO are produced per lightning flash. Our estimate of 2.6×10^{25} molecules per flash falls on the lower end of the Lawrence et al. range. Because the interferometer detects both shorter and weaker flashes compared to satellite observations or most previous ground-based observations of flashes, it is not surprising that our estimate is on the lower end. Additionally, the *Lawrence et al.* [1995] study was primarily concerned with CG lightning while the 10 July storm produced primarily IC lightning during the analysis period. IC flashes have lower peak currents ($\sim$ few kiloamps) and occur at lower air pressure and densities compared to CG lightning, and are expected to produce less NO_x per flash.

[36] The measures of lightning activity for the 10 July storm were quite variable, and this variability raises the question of whether or not the objectively analyzed lightning-produced NO_x flux is appropriately representative. Both the lightning channel-length production rate and the interferometer flash rate have minima in the early portion of the observational period and maxima in latter part of the period. The objectively analyzed NO has its peak values in the upper part of the anvil, presumably attributable to lightning-produced NO. This portion of the anvil was sampled early in the observational period, thus it may be that our analysis underestimates the lightning NO_x production. Conversely, the final pass through the anvil (the spiral pass up through the middle of the anvil that can be seen in the aircraft track in Figure 4) also showed more NO_x in the upper part of the anvil and did not detect any significant increase in NO_x compared to the earlier horizontal traversals. This suggests that the analysis has produced a reasonable estimate of the lightning-produced NO_x flux.

[37] Finally, we would like to note that the analyses that have been combined to produce the lightning production estimates are linear. Thus an error of $\pm$20% in the LNO_x production will produce a $\pm$20% error in the per channel length and per flash production estimates.

3.2. NO_x Storm Budget

[38] The ONERA lightning interferometer data span the entire lifetime of the 10 July storm. The total NO_x produced by lightning in the storm can be estimated by multiplying the NO_x production rate per unit flash by the total number of flashes, or by multiplying the production rate per meter lightning channel length by the total channel length produced over the lifetime of the storm. Using the total lightning channel length ($\sim$370,000 km) and the NO_x production rate per meter ($\sim 1.7 \times 10^{-3}$ moles/m) we compute a net production of $\sim 6.3 \times 10^5$ moles (3.8×10^{29} molecules) of NO_x. Using the total number of flashes ($\sim$5428) and the

NO_x production rate per flash ($\sim 2.6 \times 10^{25}$ molecules per interferometer flash) we compute a net production of $\sim 2.3 \times 10^5$ moles (1.4×10^{29} molecules) of NO_x.

[39] The difference between the net storm LNO_x production estimates is the result of the change in the average flash channel length over the storm lifetime; at later times the flash channels were on average longer than those measured during the observation period used to compute anvil NO_x flux, thus using the flash rate produces a lower integrated NO_x production estimate.

[40] As in the lightning analyses, the analyses that have been combined to produce the net storm LNO_x production estimates are linear. Thus an error of ±20% in the LNO_x production will produce a ±20% error in the net storm production estimate.

3.3. Global LNO_x Budgets

[41] An important goal for studies of NO_x production by lightning is to determine the contribution which lightning makes to the global nitrogen budget. Generally, two basic approaches have been used to determine a global LNO_x production rate; either an estimate of per-storm LNO_x production is multiplied by an estimate of the number of storms occurring over the globe per year [e.g., *Chameides et al.*, 1987], or an estimate of the global lightning flash count per year is multiplied by an estimate of the average LNO_x production per flash (e.g., the Flash Extrapolation Approach (FEA) reviewed by *Lawrence et al.* [1995]). Estimating global LNO_x production using the results from our study and using either of the extrapolation approaches is problematic. For example, our estimate of total storm LNO_x production ($32-88 \times 10^5$ g(N)/storm) can be combined with the commonly cited storm frequency number from *Brooks* [1925] of 16×10^6, storms/year (44,000 storms per day) to arrive at an LNO_x production rate of 52–141 Tg(N)/year. This estimate is on the high end of global LNO_x production rate estimates [see *Huntrieser et al.*, 1998], perhaps suggesting that the 10 July storm produced much more LNO_x than the average storm (it was quite long-lived and produced a large amount of lightning). Unfortunately, we have no quantitative way to normalize our LNO_x production rate for the 10 July storm without independent measures of average-storm characteristics, hence this estimate is highly uncertain. Alternatively, consider multiplying our estimate of production per flash (600 g(N)/flash) by an estimate of the global flash rate (44 ± 5 flashes/s; D. J. Boccippio, personal communication) [*Mackerras et al.*, 1998; *Williams et al.*, 2000]. This approach leads to a global production rate of 0.8 Tg(N)/year. The difficulty with this estimate is that we do not have sufficient information to relate interferometer flashes for the 10 July storm (determined in this study) with optical detector flashes (from which the global flash rate is derived). The interferometer likely sees many more flashes, and certainly many more of the weaker flashes, than the optical detectors, suggesting perhaps that this production rate estimate may be low. Thus this alternative estimate is also highly uncertain.

4. Summary and Discussion

[42] Using in situ aircraft observations, cloud model simulations, lightning interferometer observations and radar, we have produced an estimate of LNO_x (lightning-produced NO_x) production during the 10 July STERAO storm, along with estimates of average LNO_x production rate per flash, per flash channel length, and net LNO_x production over the lifetime of the storm. The production rates are computed using a control volume analysis around the storm that makes use of objectively analyzed in situ aircraft observations of NO_x flux through a control volume surface into the anvil, and cloud-model simulations that allow partitioning of the NO_x flux into an LNO_x flux and an environmental NO_x flux. The analysis reveals that approximately 60% of the NO_x passing out into the anvil was produced by lightning, with an average LNO_x flux of 11.5 moles s^{-1} (6.9×10^{24} molecules s^{-1}) during the analysis period. From the lightning interferometer data, we find that the average channel length and flash production during the analysis period was 6700 m s^{-1} and 27 flashes per second, respectively. Combining these with the LNO_x flash length production rate leads to an estimate of the average LNO_x production per meter flash channel length of 1.7×10^{-3} moles/m (or 1.0×10^{21} molecules/m). This is within the range of field estimates computed by *Stith et al.* [1999] of 2×10^{20} and 10^{22} molecules/m and the laboratory estimates computed by *Wang et al.* [1998] of between 5×10^{20} and 3×10^{21} molecules/m. The production rate per flash from our analysis is 43 moles NO_x per flash (2.6×10^{25} molecules per flash), and falls at the lower end of the estimate of *Lawrence et al.* [1995] of 0.5 to 300×10^{25} molecules per flash. The interferometer can detect both weaker flashes and flashes of shorter duration than detected by most previously used measurements systems, and the 10 July storm produced mostly IC lightning in the analysis period. Both of these considerations are consistent with the fact that our estimates of LNO_x production per flash and per unit channel length are at the low end estimates derived in previous studies.

[43] The interferometer data also provide measurements of total flashes and total flash channel length produced over the lifetime of the storm, both of which can be used to compute net storm LNO_x production. The net storm LNO_x production is estimated as $\sim 6.3 \times 10^5$ moles (3.8×10^{29} molecules) of NO_x using 3.7×10^8 meters of interferometer flash channel produced over the lifetime of the storm [*Defer et al.*, 2003]. Alternatively, we have derived a net storm LNO_x production of $\sim 2.4 \times 10^5$ moles (1.4×10^{29} molecules) of NO_x using 5428 interferometer flashes [*Defer et al.*, 2003] and our estimate of 43 moles (2.6×10^{25} molecules) per flash.

[44] The importance of LNO_x production derives from the need to understand NO_x and ozone chemistry on a global scale. The LNO_x component of global NO_x budgets have typically been derived by producing estimates of global flash rates and combining these estimates with estimates of LNO_x production per flash [e.g. *Lawrence et al.*, 1995], or by estimating per-storm LNO_x production and multiplying this by an estimate of the number of storms occurring globally in a year [*Chameides et al.*, 1987]. These global LNO_x production rates vary by more than an order of magnitude [*Liaw et al.*, 1990], and represent the largest uncertainty in the global NO_x budgets. Neither approach for producing a global budget can be directly applied using the results from this study. Problems arise from the fact that (1)

the interferometer flashes represent a new metric in LNO_x studies, and we don't have sufficient data to relate this new metric to the satellite optical flash detector counts needed for an extrapolation to the globe, and (2) we have little information that allows us to relate the 10 July storm to the average storm which is used in other estimates of global LNO_x production rates.

[45] Additional studies such as the one presented here may be able to reduce the uncertainty in LNO_x production estimates to a limited extent, but they will only apply to the particular storms being studied and extrapolation will be difficult. To make further progress we need to be able to relate the new local measurements (interferometer flashes) to existing global measurements (OTD flashes), and we need to better understand the underlying mechanisms controlling flash rates, lengths, durations, energies, and associated LNO_x production. More detailed studies of storm structure and evolution are needed, specifically with respect to the critical role storm microphysics plays in lightning generation, and these studies must encompass a variety of convective types known to be electrically active, both midlatitude and tropical in their various seasonal regimes. Our more detailed but limited observations show that the character of the lightning in individual storms can vary greatly. For example, it is well documented that continental thunderstorms produce much more lightning than maritime storms. Thus the significant uncertainty associated with studies of individual storms and the uncertainty associated with extrapolations to other storms is magnified.

[46] Another important aspect of the LNO_x budget is quantifying the vertical distribution of LNO_x sources and subsequent LNO_x transport. The general consensus on where LNO_x is deposited after its production has changed considerably over the last decade. While we have evolved from an assumption of a uniform vertical NO_x distribution to a more kinematically based assumption of a C-shaped NO_x profile, the differences in production and transport in convective storms suggest that no single generalization is applicable to all cases. For example, in the 10 July storm it appears that most of the LNO_x was transported into the anvil with little deposited below cloud base. Storms with different kinematic structures are likely to transport LNO_x to different altitudes, but until we have more observations in different type storms we cannot quantify this. In this respect it is very important to examine LNO_x production and transport by tropical storms because globally much of the earth's lightning is produced in the tropics.

[47] **Acknowledgments.** We would like to thank all those who participated in the STERAO field campaign and subsequent data analysis. This work is partially supported by NOAA CGCP award NA76GP00400. The Citation data collection and analysis were supported by the National Science Foundation through grant ATM-9634125. The National Center for Atmospheric Research is operated by the University Corporation for Atmospheric Research under the sponsorship of the National Science Foundation.

References

Bradshaw, J., D. Davis, G. Grodzinsky, R. Newell, S. Sandholm, and S. Liu, Observed distributions of nitrogen oxides in the remote free troposphere from the NASA Global Tropospheric Experiment programs, *Rev. Geophys.*, *38*, 61–116, 2000.

Brasseur, G. P., D. A. Hauglustaine, S. Walters, P. J. Rasch, J. F. Muller, C. Granier, and X. X. Tie, MOZART, a global chemical transport model for ozone and related chemical tracers: 1, Model description, *J. Geophys. Res.*, *103*, 28,265–28,289, 1998.

Brooks, C. E. P., The distribution of thunderstorms over the globe, *Meteorol. Off. Geophys. Mem., Dubl.*, *3*, 147–164, 1925.

Chameides, W. L., D. H. Stedman, R. R. Dickerson, D. W. Rusch, and R. J. Cicerone, NOx production in lightning, *J. Atmos. Sci.*, *34*, 143–149, 1977.

Chameides, W. L., D. D. Davis, J. Bradshaw, M. Rodgers, S. Sandholmm, and D. B. Bai, An estimate of the NOx production rate in electrified clouds based on NO observations from GTE/CITE 1 fall 1983 field observations, *J. Geophys. Res.*, *92*, 2153–2156, 1987.

Cressman, G. P., An operative objective analysis scheme, *Mon. Weather Rev.*, *87*, 367–374, 1959.

Defer, E., P. Blanchet, C. Thery, P. Laroche, J. E. Dye, M. Venticinque, and K. Cummins, Lightning activity for the 10 July 1996 storm during the Stratosphere-Troposphere Experiment: Radiation, aerosol, and ozone-A STERAO-A experiment, *J. Geophys. Res.*, *106*, 10,151–10,172, 1996.

Defer, E., P. Laroche, J. E. Dye, and W. Skamarock, Use of total lightning lengths to estimate NOx production in a Colorado thunderstorm, paper presented at 12th International Conference on Atmospheric Electricity, June 9 –13 , Int. Comm. on Atmos. Electr., Versailles, France, 2003.

Dye, J. E., et al., An overview of the STERAO/Deep Convection Experiment with example results from the July 10th storm, *J. Geophys. Res.*, *105*, 10,023–10,045, 2000.

Frost, G. F., et al., Photochemical ozone production in the rural southeastern United States during the 1990 Rural Oxidants in the Southern Environment (ROSE) program, *J. Geophys. Res.*, *103*, 22,491–22,508, 1998.

Huntrieser, H., H. Schlager, C. Feigl, and H. Höller, Transport and production of NO_x in electrified thunderstorms: Survey of previous studies and new observations at midlatitudes, *J. Geophys. Res.*, *103*, 28,247–28,264, 1998.

Huntrieser, H., et al., Airborne measurements of NO_x, tracer species, and small particles during the European Lightning Nitrogen Oxides Experiment, *J. Geophys. Res.*, *107*(D11), 4113, doi:10.1029/2000JD000209, 2002.

Lawrence, M. G., W. L. Chameides, P. S. Kasibhatla, H. Levy, and W. Moxim, Lightning and atmospheric chemistry: The rate of atmospheric NO production, in *Handbook of Atmospheric Electrodynamics*, vol. 1, edited by H. Holland, pp. 189–202, CRC Press, Boca Raton, Fla., 1995.

Liaw, Y. P., D. L. Sisterton, and N. L. Miller, Comparison of field, laboratory and theoretical estimates of global nitrogen fixation by lightning, *J. Geophys. Res.*, *95*, 22,489–22,494, 1990.

Mackerras, D., M. Darveniza, R. E. Orville, E. R. Williams, and S. J. Goodman, Global lightning: Total, cloud and ground flash estimates, *J. Geophys. Res.*, *103*, 19,791–19,809, 1998.

Orville, R., Spectrum of the lightning dart leader, *J. Atmos. Sci.*, *32*, 1829–1837, 1975.

Price, C., J. Penner, and M. Prather, NO_x from lightning: 1. Global distribution based on lightning physics, *J. Geophys. Res.*, *102*, 5929–5941, 1997.

Salawitch, R. J., et al., The distribution of hydrogen, nitrogen, and chlorine radicals in the lower stratosphere: Implications for changes in O_3 due to emission of NO_y from supersonic aircraft, *Geophys. Res. Lett.*, *21*, 2547–2550, 1994.

Skamarock, W. C., J. Powers, M. Barth, J. Dye, T. Matejka, D. Bartels, K. Baumann, J. Stith, D. Parrish, and G. Hubler, Numerical simulations of the 10 July STERAO/Deep Convection experiment convective system: Kinematics and transport, *J. Geophys. Res.*, *105*, 19,973–19,990, 2000.

Stith, J., J. Dye, B. Ridley, P. Laroche, E. Defer, K. Baumann, G. Hubler, R. Zerr, and M. Venticinque, NO signatures from lightning flashes, *J. Geophys. Res.*, *104*, 16,081–16,089, 1999.

Wang, Y., A. W. Desilva, G. C. Goldenbaum, and R. R. Dickerson, Nitric oxide production by simulated lightning: Dependence on current, energy, and pressure, *J. Geophys. Res.*, *103*, 19,149–19,159, 1998.

Williams, E., K. Rothkin, and D. Stevens, Global lightning variations caused by changes in thunderstorm flash rate and by changes in the number of thunderstorms, *J. Appl. Meteorol.*, *39*, 2223–2230, 2000.

World Meteorological Organization (WMO), Scientific Assessment of Ozone Depletion, 1994, WMO Global Ozone Research and Monitoring Project, Rep. 37, Geneva, 1995.

M. C. Barth, E. Defer, J. E. Dye, B. A. Ridley, W. C. Skamarock, and J. L. Stith, National Center for Atmospheric Research, P. O. Box 3000, Boulder, CO 80307, USA. (skamaroc@ucar.edu)

K. Baumann, Department of Earth and Atmospheric Sciences, Georgia Institute of Technology, Atlanta, GA 30332–0340, USA.

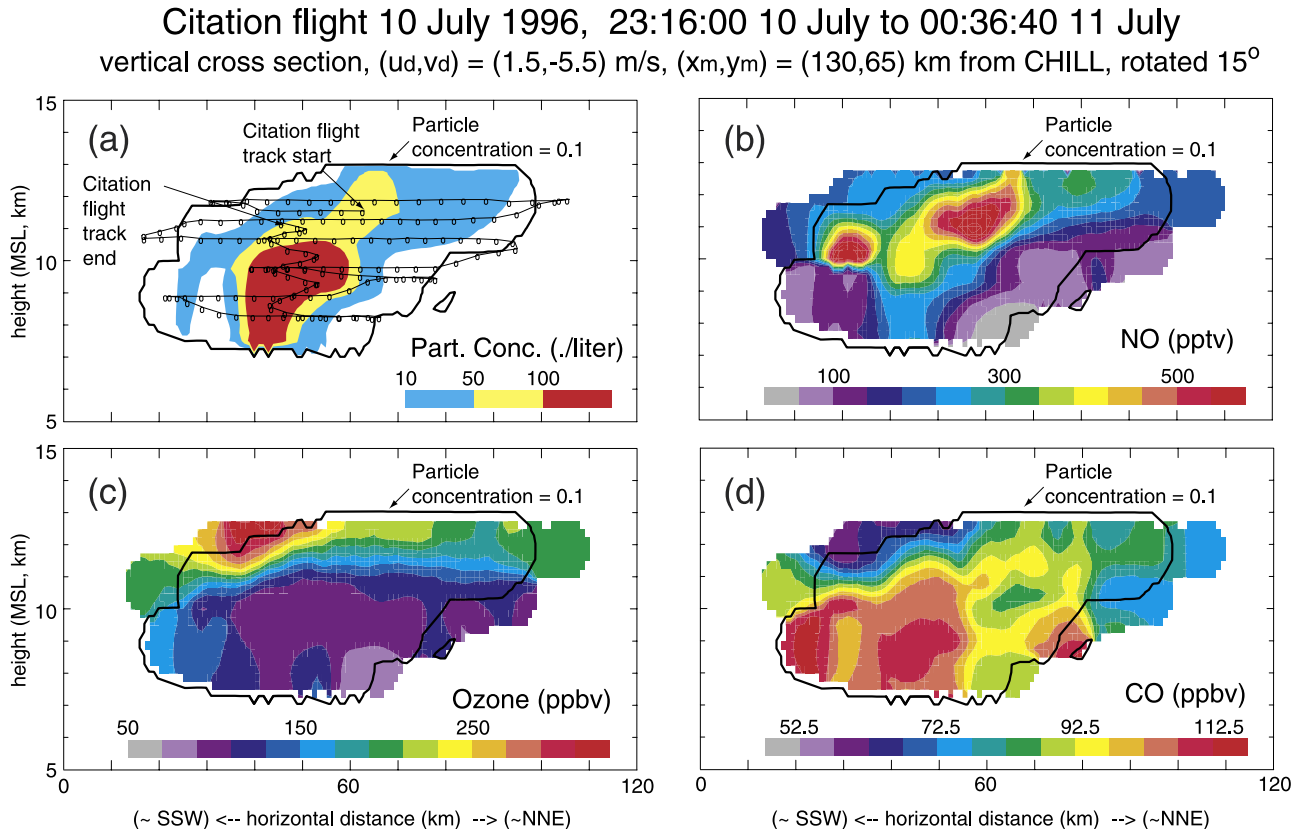

Figure 4. Objective analysis of (a) cloud particle concentration, (b) NO, (c) O_3, and (d) CO using the Citation flight data. The flight track is shown in the cloud particle concentration plot.